JOURNAL OF GEOPHYSICAL RESEARCH, VOL. 107, NO. B6, 2107, 10.1029/2001JB000197, 2002

Seismic coda attenuation after the M_w = 6.2 Armenia (Colombia) earthquake of 25 January 1999

Arantza Ugalde,[1] Carlos A. Vargas,[2] Lluís G. Pujades,[3] and José A. Canas[4]

Received 2 August 2000; revised 6 April 2001; accepted 24 April 2001; published 7 June 2002.

[1] Seismic wave attenuation in the central region of the Colombian Andes is studied using coda waves. Most of the events used occurred in the region on the occasion of the Armenia 25 January 1999 earthquake. The estimation of the decay rate of coda amplitudes (called coda Q^{-1} or Q_c^{-1}) is performed by means of the single isotropic scattering method of *Sato* [1977]. The attenuation parameters Q_i^{-1} (intrinsic absorption), Q_s^{-1} (scattering loss), and Q_t^{-1} (total attenuation) are also estimated using the multiple lapse time window method of *Hoshiba et al.* [1991]. The frequencies of interest lie between 1 and 15 Hz. Results show that scattering attenuation is predominant for the frequency bands 1.5 ± 0.5 and 13.5 ± 1.5 Hz, whereas the intrinsic absorption and scattering contribute in equal shares to total attenuation for the 3 ± 1, 5 ± 1, 7.5 ± 1.5, and 10.5 ± 1.5 Hz frequencies. A comparison among the estimated attenuation parameters indicates that Q_c^{-1} is close to total attenuation for all the studied frequency bands. On the other hand, no evidence in support of temporal changes of Q_c^{-1} before and after the main shock has been found. Finally, the regionalization of Q_c^{-1} values seems to correlate well with the geotectonic characteristics of the region. *INDEX TERMS:* 7203 Seismology: Body wave propagation; 7218 Seismology: Lithosphere and upper mantle; 9360 Information Related to Geographic Region: South America; *KEYWORDS:* Coda waves, attenuation, intrinsic and scattering Q, Colombia

1. Introduction

[2] On 25 January 1999 a M_w = 6.2 earthquake struck the coffee-growing region of western Colombia. This earthquake has caused more damage than any other seismic event in Colombia this century. The most affected cities were Armenia and Pereira, where extensive damage occurred. Although this region has experienced several destructive earthquakes in the past, the great damage caused by this moderate size earthquake is probably due to soil amplification phenomena, enhanced by the topographic shapes of the land, the presence of deep layers of volcanic ash, and the volcanic sedimentary deposits as well as man-made fill soft soils. Moreover, heavy damages occurred because many of the structures were built before the 1984 national earthquake resistant construction code was issued.

[3] The earthquake occurred in the central mountain range, the Cordillera Central, of three north trending mountain ranges of northern Andes in western Colombia (Figure 1). This mountain range has active volcanoes, and the epicenter was located near the Ruiz-Tolima volcanic complex. The volcanic activity of this region is associated with the subduction of the Nazca tectonic plate beneath South America, and therefore most earthquakes in this zone are at least 100 km beneath the surface. This earthquake, however, probably occurred at a depth of ~17 km on a fault called Cauca-Almaguer, which is part of the Romeral fault system, and was caused by some crustal adjustment of the local fault systems. The earthquake source parameters are available at *National Earthquake Information Center* (*NEIC*) [1999].

[4] From the tectonic and seismological point of view the central region of the Colombian Andes is a well-monitored zone [e.g., *Taboada et al.*, 1998]. However, although the coffee-growing region is a very active area capable of generating moderate size earthquakes, there is a lack of measurements of seismic wave attenuation. Previous studies have been done in the specific zone of Nevado del Ruiz volcano concerning tomography [*Muñoz*, 1992] and temporal variations in Q_c [*Londoño*, 1996; *Londoño et al.*, 1998].

[5] Coda waves have been proven to be a useful tool to study the source spectrum and the propagation properties of seismic waves [*Aki*, 1980, 1982]. Particularly, the decay rate of the coda amplitudes Q_c^{-1} has been widely used to characterize seismic wave attenuation in the Earth's lithosphere in different regions of the world. The knowledge of regional values of Q_c and its spatial variation attracts considerable interest in relation to tectonics and seismicity, being an important subject in seismic risk analysis and engineering seismology [*Singh and Herrmann*, 1983; *Jin and Aki*, 1988]. Q_c^{-1} can be estimated using methods based on the single scattering model for coda wave generation [*Aki and Chouet*, 1975; *Sato*, 1977] which are based on the fit of the seismogram envelope, obtained at different frequency bands, to single-scattering theoretical models.

[6] On the other hand, multiple-scattering models are needed in order to separate the two different loss mechanisms of seismic wave attenuation: intrinsic absorption and scattering. The inverse quality factors Q_t^{-1}, Q_i^{-1}, and Q_s^{-1} characterize total attenuation (defined as the fraction of energy lost during a wave cycle), intrinsic absorption (caused by the conversion of seismic energy into heat), and scattering attenuation, (due to the redistribution of energy that occurs when seismic waves interact with the heterogeneities of the medium), respectively. These parameters are related by the equation $Q_t^{-1} = Q_i^{-1} + Q_s^{-1}$ [*Dainty*, 1981].

[7] Within the framework of the single-scattering theory, Q_c^{-1} represents the effective (total) attenuation. Nevertheless, as summarized by *Aki* [1991], some theoretical and experimental model studies have confirmed that Q_c^{-1} measures only the intrinsic

[1]Observatori de l'Ebre, Roquetes, Spain.
[2]Ingeominas, Manizales, Colombia.
[3]Departament Enginyeria del Terreny i Cartogràfica, Universitat Politècnica de Catalunya, Barcelona, Spain.
[4]Instituto Geográfico Nacional, Madrid, Spain.

0148-0227/02/2001JB000197$09.00

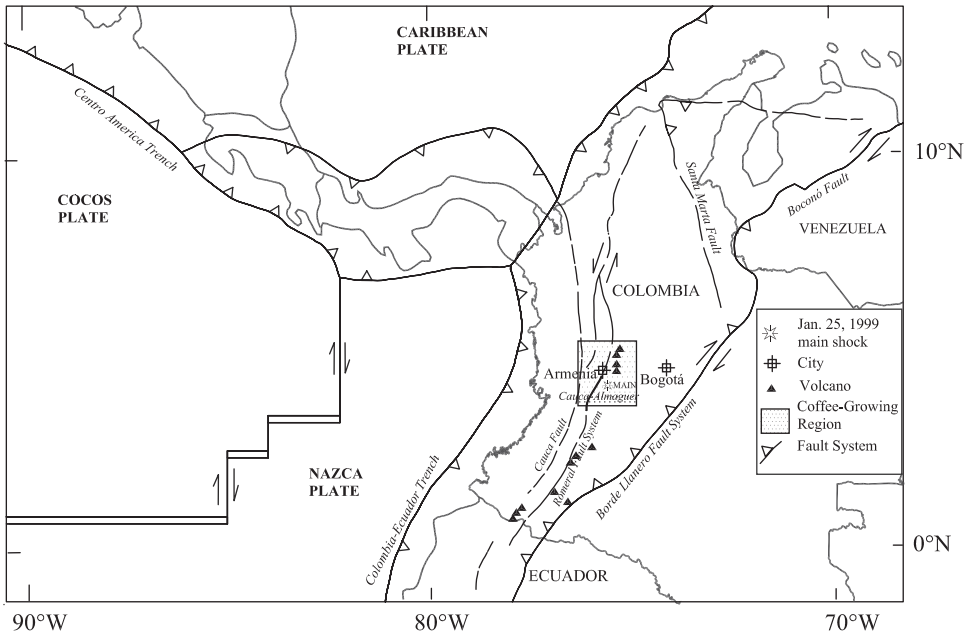

Figure 1. Tectonic framework of the northern Andes region and study area. The Cordillera Central runs along the SW-NE axis, extending between the Colombia-Ecuador trench and the Borde-Llanero fault system. The location of the 25 January 1999 earthquake is shown.

absorption. On the other hand, the field observations that have been carried out in different regions of the world [e.g., *Canas et al.*, 1998; *Jin et al.*, 1994] have shown that in general, Q_c^{-1} is bounded between Q_i^{-1} and Q_t^{-1}. In this study, we will estimate Q_c^{-1} and its frequency dependence in the central region of the Colombian Andes by means of the single isotropic scattering (SIS) model [*Sato*, 1977]. We will also analyze the contribution of intrinsic absorption and scattering to total attenuation in the region by means of the multiple lapse time window analysis (MLTWA) method [*Hoshiba et al.*, 1991]. The obtained Q parameters are discussed, and we correlate the results with the seismotectonics of the region.

2. Data

[8] For this study, 314 good quality seismograms from 48 earthquakes recorded by 14 short-period seismic stations were available. Stations consist of three-component sensors with a natural frequency of 1 Hz installed on hard rock. Twelve of the stations belong to the local network deployed for monitoring the Ruiz-Tolima volcanic complex, and the remaining two (PACO and PERE) are part of a regional seismic monitoring system (Table 1 and Figure 2). The stations are configured for a continuous analog transmission of waveform data to the central station located in the city of Manizales, where they are digitized at a rate of 100 samples per second using a 20-bit scheme. The velocity response of the whole system is flat between 1 and 15 Hz.

[9] Earthquakes used have focal depths <295 km and local magnitudes range between 2.0 and 4.1. They are associated with the main tectonic features of the region: the subduction of the Nazca plate beneath South America, which induces intermediate depth events; and the Romeral fault system responsible for the shallow seismicity which caused the last Armenian earthquake. Twenty-eight events which occurred after the 25 January earthquake and 20 earthquakes happened earlier in this region were analyzed (Table 2 and Figure 2). Unfortunately, the short dynamic range of the stations together with the short relative distance between the local network and the main shock hypocenter do not allow to analyze the recordings of the 25 January earthquake.

3. Methods

3.1. The SIS Model

[10] The single backscattering model of *Aki and Chouet* [1975] has been widely used to estimate the decay rate of the coda amplitudes Q_c^{-1}, as summarized by *Herráiz and Espinosa* [1987]. However, the model assumes that the source of the earthquake and the receiver are coincident so it holds, empirically, for $t > 2t_S$, where t_S is the S wave travel time [*Rautian and Khalturin*, 1978]. Therefore it is sometimes difficult to use the available seismic records for the coda analysis when recording times are short or when the signal-to-noise ratio is low. The *Sato* [1977] single isotropic scattering model, which is an extension to the S-S single scattering model of *Aki and Chouet* [1975], considers the case of noncoincident source and receiver, thus allowing one to begin the coda analysis just after the S wave arrival. In this model,

Table 1. List of the 14 Seismic Stations Used With Their Geographical Coordinates

Station Code	Longitude, °N	Latitude, °W	Height, m
ALF2	4.869	75.340	4760
BIS1	4.894	75.339	5030
CALA	4.535	75.618	2240
NCIS	4.847	75.349	4665
GUAY	4.455	75.620	2750
ISTM	4.695	75.330	3900
NIDO	4.664	75.327	4715
OLLE	4.902	75.359	4660
PERE	4.861	75.723	1300
PACO	5.493	75.456	2200
RECI	4.867	75.304	4600
REF3	4.901	75.347	4743
RODE	4.490	75.392	2750
TOLD	4.943	75.399	3760

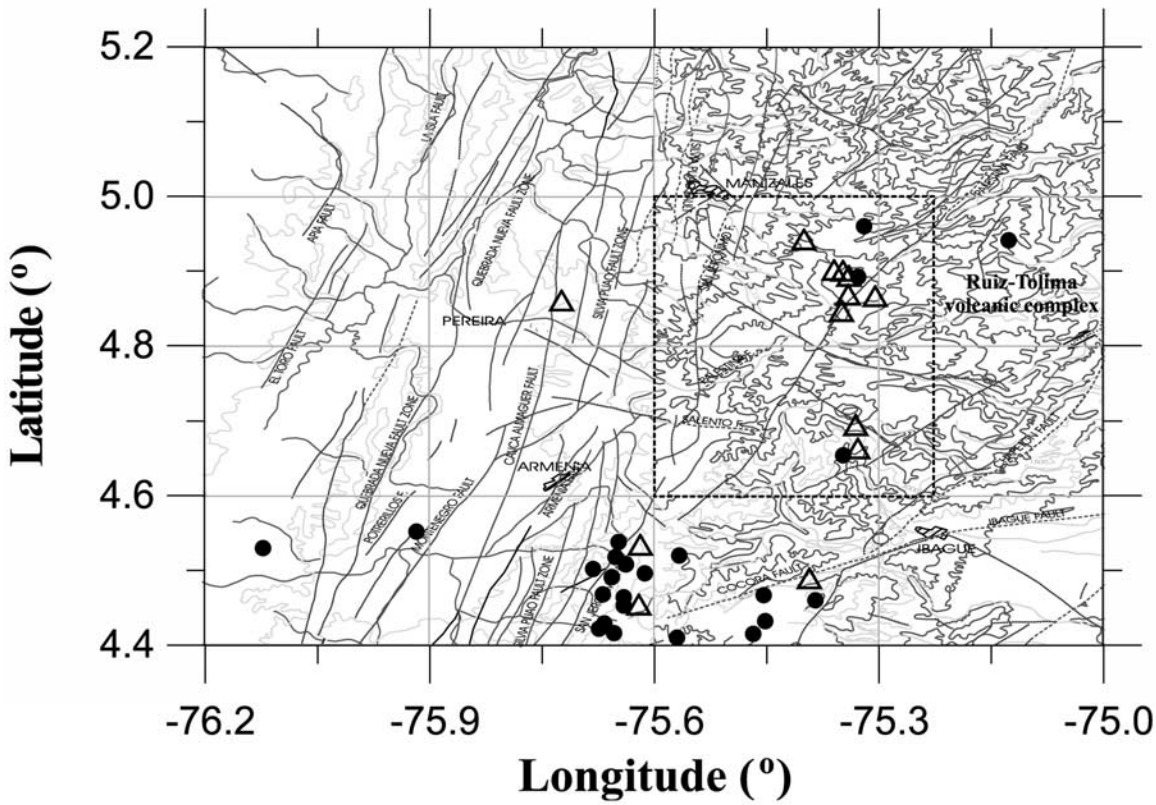

Figure 2. Detailed map of part of the studied region. The main faults and the location of the Ruiz-Tolima volcanic complex (rectangular area surrounded by dashed square) are shown together with the location of some of the stations (triangles) and earthquakes (solid circles) used. See color version of this figure at back of this issue.

spherical radiation and isotropic scattering are assumed, and the random distribution of scatterers is considered to be homogeneous and isotropic.

[11] According to *Sato* [1977] the coda energy density at frequency f can be expressed as

$$E_s(f|r,t) = \left[W_0(f)g_0(f)/4\pi r^2\right]K(a)\exp\left[-2Q_c^{-1}\pi ft\right], \qquad (1)$$

where r is the hypocentral distance; t is the lapse time measured from the origin time of the earthquake; W_0 is the total energy radiated from the source; g_0 is the total scattering coefficient; $K(a) = (1/a)\ln[(a+1)/(a-1)]$, $(a > 1)$; and $a = t/t_S$. Taking into account that energy density is proportional to the mean square amplitudes of coda waves, taking natural logarithms of equation (1) and rearranging terms, we get

$$\ln[A_{\rm obs}(f|r,t)/k(r,a)] = \ln C(f) - (\pi f/Q_c)t, \qquad (2)$$

where $A_{\rm obs}(f|r, t)$ represent the observed root-mean-square (RMS) amplitudes of the narrow band-pass-filtered waveforms with center frequency f; $k(r, a) = (1/r)\ K(a)^{0.5}$; and $C(f)$ is a constant. The attenuation of coda waves, Q_c^{-1}, can be easily obtained from the slope of the straight line fitting the measured ln $[A_{\rm obs}(f|r, t)/k(r, a)]$ versus t for a given center frequency.

3.2. The MLTWA Method

[12] The multiple lapse time window method [*Hoshiba et al.*, 1991] has been applied and described in several papers [e.g., *Fehler et al.*, 1992; *Mayeda et al.*, 1992; *Jin et al.*, 1994; *Pujades et al.*, 1997; *Canas et al.*, 1998; *Ugalde et al.*, 1998]. It consists of comparing the predicted seismic energy by the multiple isotropic scattering theory in several lapse time windows measured from the S wave onset as a function of hypocentral distance, with the observations. Thus two attenuation parameters are calculated [*Wu*, 1985]: the seismic albedo (B_0), defined as the dimensionless ratio of scattering loss to total attenuation, and the inverse of the extinction length L_e^{-1} that is the inverse of the distance (in kilometers) over which the primary S wave energy is decreased by e^{-1}. The total attenuation, scattering loss, and intrinsic absorption parameters are then calculated through the expressions $Q_t^{-1} = L_e^{-1}\beta/\omega$, $Q_s^{-1} = B_0 Q_t^{-1}$, and $Q_i^{-1} = (1 - B_0)\ Q_t^{-1}$, where ω is the angular frequency and β is the shear wave velocity [*Hoshiba et al.*, 1991].

[13] The model curves of the energy density at a given lapse time and hypocentral distance, under the assumptions of multiple isotropic scattering and uniform distribution of scatterers, are calculated by means of the following integral equation [*Zeng et al.*, 1991]:

$$E(\mathbf{r},t) = E_0\left(t - \frac{|\mathbf{r}-\mathbf{r}_0|}{\beta}\right)\frac{e^{-L_e^{-1}|\mathbf{r}-\mathbf{r}_0|}}{4\pi|\mathbf{r}-\mathbf{r}_0|^2} + \int_V g\,E\left(\mathbf{r}_1, t - \frac{\mathbf{r}_1-\mathbf{r}}{\beta}\right)\frac{e^{-L_e^{-1}|\mathbf{r}_1-\mathbf{r}|}}{4\pi|\mathbf{r}_1-\mathbf{r}|^2}dV_1, \qquad (3)$$

where E($\mathbf{r}$, t) is the seismic energy density per unit volume at position $\mathbf{r}$ and time t for a point source at $t = 0$ located at $\mathbf{r}_0$. The first term on the right-hand side of equation (3) represents the direct wave energy traveling from the source located at $\mathbf{r}_0$ to the receiver located at $\mathbf{r}$, and the second term is the contribution of all

Table 2. Events Used in the Analysis[a]

Date	Origin Time, UT	Latitude, °N	Longitude, °W	Depth, km	M_L
1 Dec. 1998	0226:30.42	7.11	72.92	163.7	2.1
3 Dec. 1998	1627:54.13	3.61	75.69	53.7	2.4
7 Dec. 1998	2136:37.34	4.70	76.40	104.5	3.8
9 Dec. 1998	2015:20.65	6.99	73.08	138.2	2.3
10 Dec. 1998	0545:31.61	6.50	76.77	114.9	3.5
19 Dec. 1998	0840:46.06	4.65	75.35	0.1	2.9
23 Dec. 1998	1006:54.58	4.53	76.12	106.4	2.5
24 Dec. 1998	2316:55.50	5.57	75.24	99.0	3.7
25 Dec. 1998	0944:49.03	5.29	76.04	131.6	2.1
28 Dec. 1998	0603:41.07	6.90	72.90	48.3	4.1
30 Dec. 1998	0516:36.53	5.49	76.38	77.1	2.8
13 Jan. 1999	1914:16.16	6.40	73.40	252.4	2.2
15 Jan. 1999	0023:50.10	5.85	72.63	1.0	2.3
15 Jan. 1999	1053:47.37	7.07	73.24	141.5	2.4
16 Jan. 1999	1119:51.30	6.80	72.74	56.0	2.4
17 Jan. 1999	0125:56.76	5.80	73.53	38.0	2.2
17 Jan. 1999	0125:57.40	5.77	73.56	35.5	2.2
20 Jan. 1999	1412:16.02	4.96	75.32	138.3	3.3
23 Jan. 1999	0420:18.40	6.04	74.50	80.7	2.4
24 Jan 1999	1305:03.52	7.01	74.73	113.6	3.1
1 Feb. 1999	0323:35.20	4.94	75.13	63.0	2.0
2 Feb. 1999	0543:11.50	6.42	72.69	151.6	2.2
2 Feb. 1999	0713:00.08	2.31	75.72	35.1	2.0
2 Feb. 1999	0934:06.65	4.26	75.16	14.3	2.1
2 Feb. 1999	1012:23.15	4.45	75.64	13.3	2.0
2 Feb. 1999	1205:01.45	4.47	75.45	31.0	2.1
2 Feb. 1999	1206:57.76	4.50	75.61	15.9	2.0
2 Feb. 1999	1219:58.32	4.41	75.57	30.2	2.1
2 Feb. 1999	1309:33.06	4.43	75.45	28.2	2.2
2 Feb. 1999	1400:20.83	4.46	75.39	30.9	2.0
2 Feb. 1999	1715:43.01	4.42	75.65	14.5	2.2
2 Feb. 1999	2108:59.18	4.55	75.92	35.8	2.1
2 Feb. 1999	2135:18.75	4.52	75.57	22.2	2.0
2 Feb. 1999	2215:01.16	4.54	75.65	11.1	2.0
3 Feb. 1999	0029:13.40	4.41	75.47	29.3	2.2
3 Feb. 1999	1447:43.46	4.89	75.25	16.3	2.2
3 Feb. 1999	1452:04.25	4.11	75.33	0.7	2.1
3 Feb. 1999	1506:06.73	4.52	75.65	7.7	2.1
3 Feb. 1999	1510:44.76	4.43	75.67	5.3	2.1
4 Feb. 1999	0532:51.37	4.50	75.68	27.9	2.8
4 Feb. 1999	1841:03.81	7.97	74.59	49.4	2.0
6 Feb. 1999	2126:36.39	4.46	75.64	20.2	2.1
8 Feb. 1999	0001:58.61	7.17	73.58	214.1	2.2
9 Feb. 1999	2323:48.30	4.49	75.66	13.1	2.2

[a] The origin date and time, geographical location, and local magnitude are presented for the 48 earthquakes analyzed.

orders of scattered energy from all possible scatterers located at $\mathbf{r}_1$; $g = L_e^{-1}B_0$ is the scattering coefficient. A solution of equation (3) in the integral transform domain is given by *Zeng et al.* [1991]. A numerical solution for the theoretical function $E(r, t)$ that represents the energy received at hypocentral distance r and time t for various combinations of L_e^{-1} and B_0 can also be obtained by using a hybrid method that consists of combining analytical solutions for single scattering with a numerical solution based on the two-dimensional fast Fourier transform for multiple scattering [*Sato*, 1994].

4. Data Analysis and Results

4.1. Q_c^{-1}

[14] Prior to analysis a visual inspection of all the data was performed in order to discard those seismograms or portions of seismograms with spurious signals, digital glitches, clipped events, or poor signal-to-noise ratios. For this study, only the vertical components were used because it has been shown that the coda analysis is independent of the component of the particle ground motion [e.g., *Hoshiba*, 1993]. Then each seismogram was band-pass-filtered over the frequency bands 1–2 (1.5 ± 0.5) Hz, 2–4 (3 ± 1) Hz, 4–6 (5 ± 1) Hz, 6–9 (7.5 ± 1.5) Hz, 9–12 (10.5 ± 1.5) Hz, and 12–15 (13.5 ± 1.5) Hz, using eight-pole Butterworth filters. From the band-pass-filtered data the RMS amplitudes were calculated by using a time window length for the averaging of $t \pm 2$ s for the frequency band centered at 1.5 Hz and $t \pm 1$ s for the 3, 5, 7.5, 10.5, and 13.5 center frequencies, both time windows spaced 0.5 s. We chose a 10-s length noise sample before the P wave onset so that only the amplitudes with a signal-to-noise ratio greater than 2 were considered for the calculations. The parameters Q_c^{-1} for each epicenter-station path were finally obtained by performing a least squares regression applied to equation (2) for which a 20-s time window on the linear part of ln $[A_{\text{obs}}(f|r, t)/k(r, a)]$ was chosen. An example of the procedure for an actual seismogram is shown in Figure 3. All the estimated values and averages are plotted in Figure 4, where each small circle represents Q_c^{-1} from a single seismogram. It was not possible to determine Q_c^{-1} for all event-station-frequency band combinations because of different noise conditions and sizes of the events. Moreover, the monotonous amplitude decay of the coda may be occasionally disturbed by the presence of reflected phases. In order to automate the process, an arbitrary threshold value of 0.85 for the correlation coefficient was adopted so that only the Q_c^{-1} values obtained with

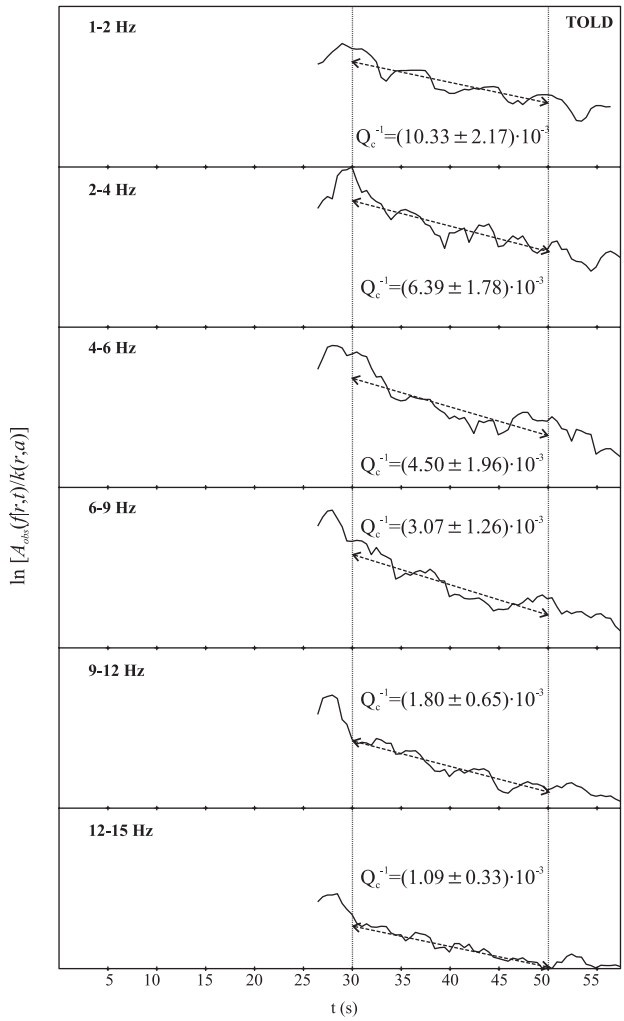

Figure 3. Example of the function ln $[A_{\mathrm{obs}}(f|r, t)/k(r, a)]$ versus lapse time t for the earthquake occurred on 7 December 1998, 2136:37.34 UT and recorded by station TOLD. The 20-s time intervals used for the linear regression, and the obtained slopes are shown.

correlation coefficients greater than 0.85 were kept. We tested that using the 0.85 value, <5% of data were rejected. The average numerical values and their associated standard deviations are listed in Table 3.

[15] Figure 4 shows a scatter in the Q_c^{-1} values for each frequency band that may be due not to errors in the analysis but to different sampling regions of coda waves during their propagation, indicating that there may exist lateral variations in the attenuation properties of the lithosphere in the studied region. Fitting the Q_c^{-1} data in Table 3 to the frequency law $Q_c^{-1}(f) = Q_0^{-1} f^{-\nu}$, we obtain that $Q_0^{-1} = (23.06 \pm 0.96) \times 10^{-3}$ and $\nu = 1.10 \pm 0.05$.

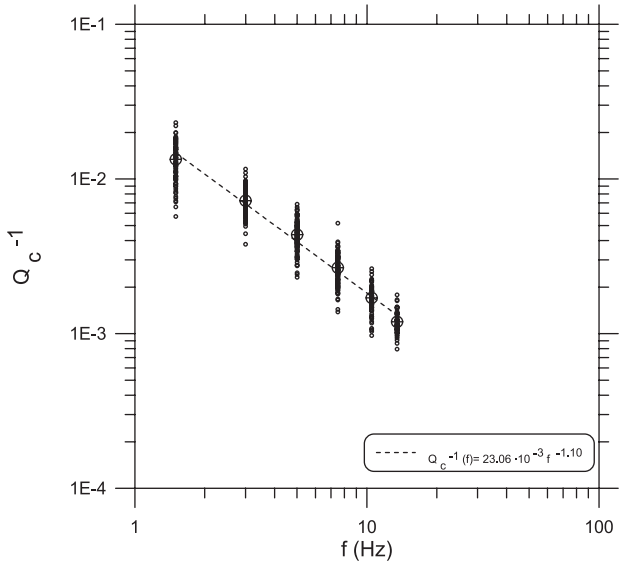

Figure 4. Q_c^{-1} as a function of frequency for the 1–2, 2–4, 4–6, 6–9, 9–12, and 12–15 Hz studied frequency bands. The small circles that correspond to a Q_c^{-1} estimate for a single seismogram and the weighted mean for each frequency band are plotted.

4.2. Temporal Changes in Q_c^{-1}

[16] Some observational studies have found evidences for significant temporal variations in Q_c^{-1} before and after some major earthquakes [e.g., *Jin and Aki*, 1989]. Recently, *Hiramatsu et al.* [2000] confirmed temporal variations in Q_c^{-1} and b value in Japan and concluded that Q_c^{-1} can be a reliable indicator of stress changes in the crust if stable estimations are performed using a large number of stations. Also *Londoño* [1996] and *Londoño et al.* [1998], who studied the Nevado del Ruiz volcano (which is part of the study area in the present work), reported significant changes in Q_c^{-1} related to the level of volcanic activity. These observations suggest that Q_c^{-1} may be used as an empirical tool for earthquake prediction. There are also some extensive studies which have obtained negative results when studying temporal changes in Q_c^{-1} [e.g., *Aster et al.*, 1996; *Antolik et al.*, 1996]. In this study, we also examined the possibility of a temporal change in Q_c^{-1} by measuring the coda decay rates for the earthquakes occurring before and after the 25 January main shock, separately. Comparing the Q_c^{-1} numerical values listed in Table 3 (second and third columns) and taking into account the corresponding error bars, we

Table 3. Mean Values of Coda Attenuation for All the Studied Frequency Bands[a]

Center Frequency, Hz	Q_c^{-1}				
	All Data	Before 25 Jan.	After 25 Jan.	r ≥ 100 km	r > 100 km
1.5	$(13.41 \pm 3.56) \times 10^{-3}$	$(13.98 \pm 3.42) \times 10^{-3}$	$(11.21 \pm 3.34) \times 10^{-3}$	$(10.29 \pm 2.22) \times 10^{-3}$	$(13.71 \pm 3.53) \times 10^{-3}$
3.0	$(7.24 \pm 1.38) \times 10^{-3}$	$(7.59 \pm 1.37) \times 10^{-3}$	$(6.38 \pm 1.02) \times 10^{-3}$	$(5.68 \pm 0.58) \times 10^{-3}$	$(7.41 \pm 1.34) \times 10^{-3}$
5.0	$(4.36 \pm 0.91) \times 10^{-3}$	$(4.47 \pm 0.91) \times 10^{-3}$	$(4.15 \pm 0.89) \times 10^{-3}$	$(3.71 \pm 0.95) \times 10^{-3}$	$(4.42 \pm 0.88) \times 10^{-3}$
7.5	$(2.67 \pm 0.58) \times 10^{-3}$	$(2.73 \pm 0.48) \times 10^{-3}$	$(2.53 \pm 0.72) \times 10^{-3}$	$(2.25 \pm 0.46) \times 10^{-3}$	$(2.75 \pm 0.57) \times 10^{-3}$
10.5	$(1.70 \pm 0.32) \times 10^{-3}$	$(1.71 \pm 0.32) \times 10^{-3}$	$(1.65 \pm 0.30) \times 10^{-3}$	$(1.52 \pm 0.22) \times 10^{-3}$	$(1.73 \pm 0.32) \times 10^{-3}$
13.5	$(1.19 \pm 0.20) \times 10^{-3}$	$(1.21 \pm 0.19) \times 10^{-3}$	$(1.15 \pm 0.20) \times 10^{-3}$	$(1.12 \pm 0.16) \times 10^{-3}$	$(1.21 \pm 0.20) \times 10^{-3}$

[a] Estimates of Q_c^{-1} using all the available data, results for the events occurred before and after the 25 January 1999 Armenia earthquake, and the estimates for hypocentral distances less and greater than 100 km are presented.

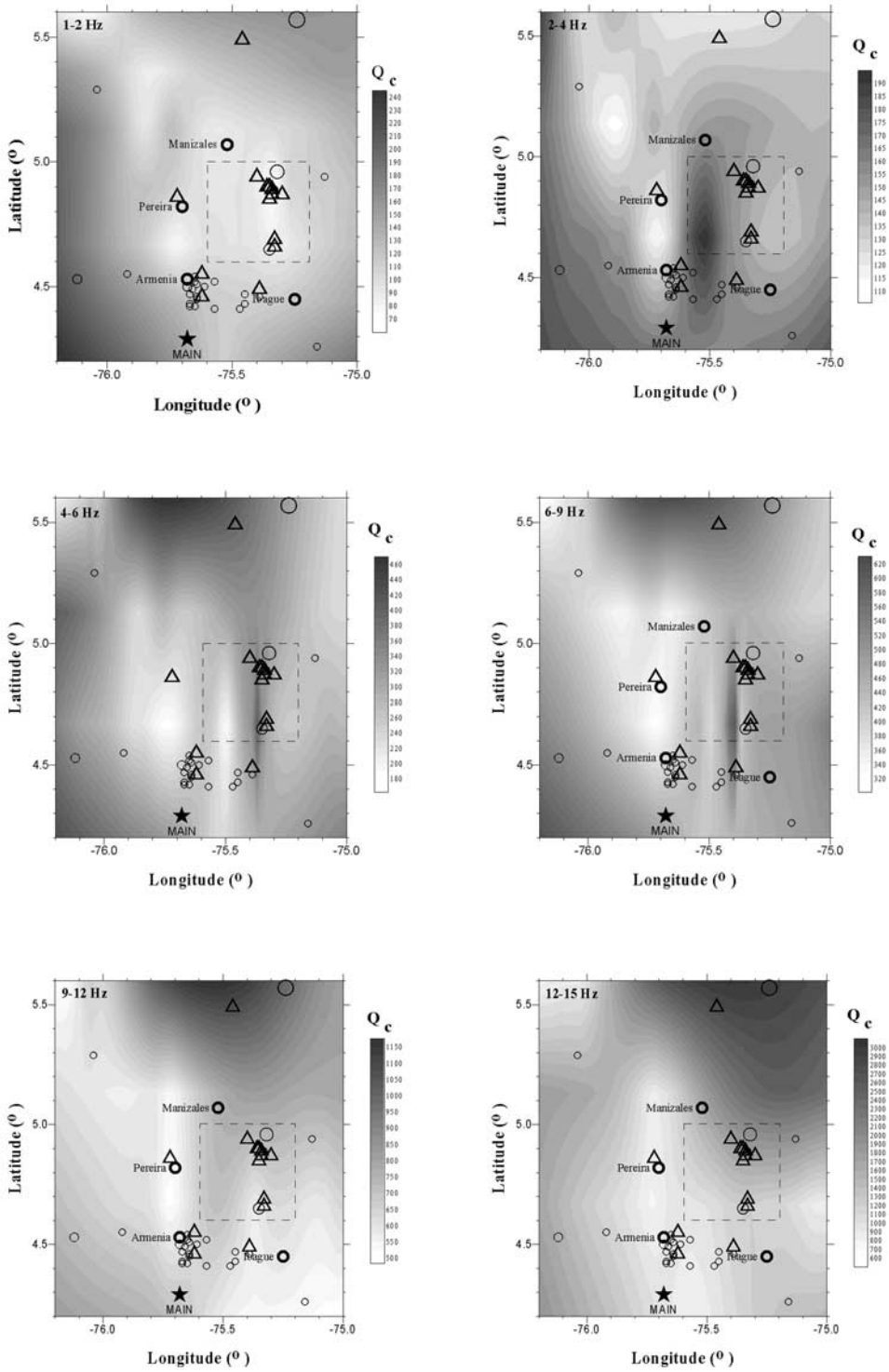

Figure 5. Regionalization of Q_c using the method of the midpoints of the epicenter-station paths. The iso-Q_c contour maps for all the studied frequency bands are plotted. Shepard's method (inverse distance weighted least squares) has been used for the data interpolation. The dashed squares surround the Ruiz-Tolima volcanic complex area.

can observe no significant differences between the Q_c^{-1} estimates for the two cases considered.

4.3. Spatial Variations of Q_c^{-1}

[17] Seismic attenuation also varies spatially. It is well known that the coda is composed of scattered waves in an ellipsoidal volume so they represent an average over a large region. The lapse time is related to the region of sampling [*Pulli*, 1984]. Because of the geographical distribution of earthquakes and stations in the study region we are measuring the coda decay at both short and long lapse times (short and long hypocentral distances). For this reason, two zones of activity were defined ($r \leq 100$ km and

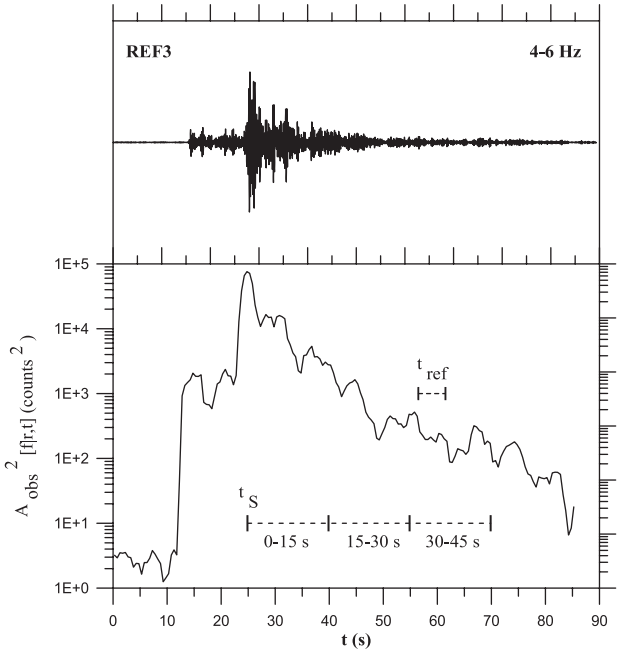

Figure 6. (top) Example of the 4–6 Hz band-pass-filtered seismogram from station REF3 (origin date and time are 11 February 1999, 0314:02.29 UT). (bottom) Mean square amplitude showing the three consecutive time windows used for integrating energy and the reference time window considered.

r > 100 km) and Q_c^{-1} was examined. Table 3 shows the Q_c^{-1} values obtained for the two zones considered and all the studied frequency bands. Given the confidence bounds, no significant differences between the attenuation for long and short lapse times are observed.

[18] On the other hand, we performed a regionalization of Q_c data in order to relate the obtained Q_c values to different tectonic characteristics of the region. We used the method proposed by *Singh and Herrmann* [1983], who plotted a contour map of Q_c for the United States. Figure 5 shows the contour map of part of the studied region for all the studied frequency bands. For plotting this map we first assigned each estimated Q_c value to the midpoint of the epicenter-station path, and then we performed an inverse distance weighted least squares interpolation (Shephard's method) of the data. We have to say that because of the distribution of stations and earthquakes the spatial resolution was poor for distant events so we limited the map to ~100 km of epicentral distance. From Figure 5 a relation between the Q_c values and the geotectonic characteristics of the region such as faulting areas and the location of the Ruiz-Tolima volcanic complex may be inferred. We will discuss it in section 5.

4.4. Estimation of Q_i^{-1}, Q_s^{-1}, and Q_t^{-1}

[19] The model parameters (L_e^{-1}, B_0) were estimated following the MLTW method [*Hoshiba et al.*, 1991]. For the calculation of the observed seismic energies as a function of hypocentral distance we first computed the RMS amplitudes of the band-pass-filtered waveforms as a function of lapse time t as we described in section 4.1. Then we integrated the function $A_{obs}^2(f|r, t)$ over the three consecutive time windows: 0–15, 15–30, and 30–45 s measured from the S wave onset, and we obtained the energies represented by the function $e_i^{obs}(f|r)$ (I = 1, 2, 3). Figure 6 shows an example of the processing for a seismogram recorded at station REF3. The coda normalization technique [*Aki*, 1980] was then applied to correct for different earthquake sources and site amplification factors. The normalized observed seismic energies for the center frequency f and the ith time window $E_i^{obs}(f|r)$ (I = 1, 2, 3) were calculated by computing the ratio $e_i^{obs}(f|r)/A_{obs}^2(f|r, t_{ref})$ (I = 1, 2, 3), where the reference time window t_{ref} must satisfy the condition $t_{ref} > 2r/\beta$ for all hypocentral distances. We chose a 5-s-long time window centered at 59 s past the origin time of the earthquake. Because the shear wave velocity in this region is considered to be β = 3.4 km s^{-1} [*Coral*, 1987], this means that all the earthquakes with hypocentral distances up to 100 km were used in the analysis. The small magnitude of most of the events, which makes the signal to be buried in the noise at long travel times, determined the choice of the reference time window. Data with amplitudes of less than twice the amplitude of a noise sample of length 10 s prior to the P wave arrival were discarded. Finally, we multiplied the function $E_i^{obs}(f|r)$ (I = 1, 2, 3) by r^2 to perform a correction for the geometrical spreading effect. It only applies to body waves in a uniform medium.

[20] The theoretical energy-distance $E_i^{syn}(f|r)$ (I = 1, 2, 3) curves for each 0–15, 15–30, and 30–45 s time window from the S wave arrival were calculated by solving equation (3) numerically. The synthetics were also corrected for the geometrical spreading effect and normalized using the same processing as for the observed data.

[21] To find the best fit model parameters L_e^{-1} and B_0, we performed a multiple least squares regression between the observed and synthetic data. The F distribution test was used to plot the confidence contour for the estimated model parameters using [*Draper and Smith*, 1981]

$$S(\boldsymbol{\theta}) = S(\hat{\boldsymbol{\theta}})\left[1 + \frac{p}{n-p}F(p, n-p, 1-\alpha)\right], \qquad (4)$$

where $S(\hat{\theta})$ is the minimum value of $S(\boldsymbol{\theta})$ defined as

$$S(\boldsymbol{\theta}) = 1n\sum_{i=1}^{3}\sum_{j=1}^{n}\left\{\log_{10}\left(r^2E_{in}^{obs}\right) - \log_{10}\left[r^2E_{in}^{syn}(\boldsymbol{\theta})\right]\right\}^2. \qquad (5)$$

The number of model parameters is p = 2 ($\boldsymbol{\theta} = L_e^{-1}, B_0$), n is the number of observations, F is the Fisher distribution function, and 100(1 − α)% is the confidence value which was chosen to be α = 0.05. Equation (5) was calculated for each pair (L_e^{-1} = 0.001, 0.002,. . ., 0.010 km^{-1}; B_0 = 0.02, 0.04,. . ., 1.0) and for all the analyzed frequency bands. Figure 7 shows the best fitting energy-distance curves along with the observed data for each studied frequency band. Table 4 contains the estimated attenuation parameters L_e^{-1}, B_0, Q_i^{-1}, Q_s^{-1}, and Q_t^{-1}. The ratios $S(\boldsymbol{\theta})/S(\hat{\boldsymbol{\theta}})$ are plotted in Figure 8, where the unshaded zones correspond to the 95% confidence areas. The errors associated to L_e^{-1} and B_0 (Table 4) are not symmetric because of the asymmetry of the confidence areas (Figure 8).

[22] Fitting the estimated parameters in Table 4Q_i^{-1} (intrinsic absorption), Q_s^{-1} (scattering attenuation) and Q_t^{-1} (total attenuation) to the frequency law $Q^{-1}(f) = Q_0^{-1}f^{-\nu}$, we obtained that $Q_{0i}^{-1} = (5.45 \pm 0.92) \times 10^{-3}$, $\nu_I = 0.99 \pm 0.09$; $Q_{0s}^{-1} = (6.68 \pm 1.64) \times 10^{-3}$, $\nu_s = 1.02 \pm 0.13$; and $Q_{0t}^{-1} = (12.38 \pm 1.32) \times 10^{-3}$, $\nu_l = 1.02 \pm 0.13$.

5. Discussion and Conclusions

[23] In this study, average values of the attenuation parameters Q_c^{-1}, Q_i^{-1}, Q_s^{-1}, and Q_t^{-1} have been estimated for the coffee-growing region of western Colombia. Table 4 shows that the seismic albedo is >0.5 for two frequency bands centered at 1.5 and 13.5 Hz, which indicates that scattering is the predominant attenuation effect in the region at the scale length of these frequencies. On the contrary, given the confidence bounds, the

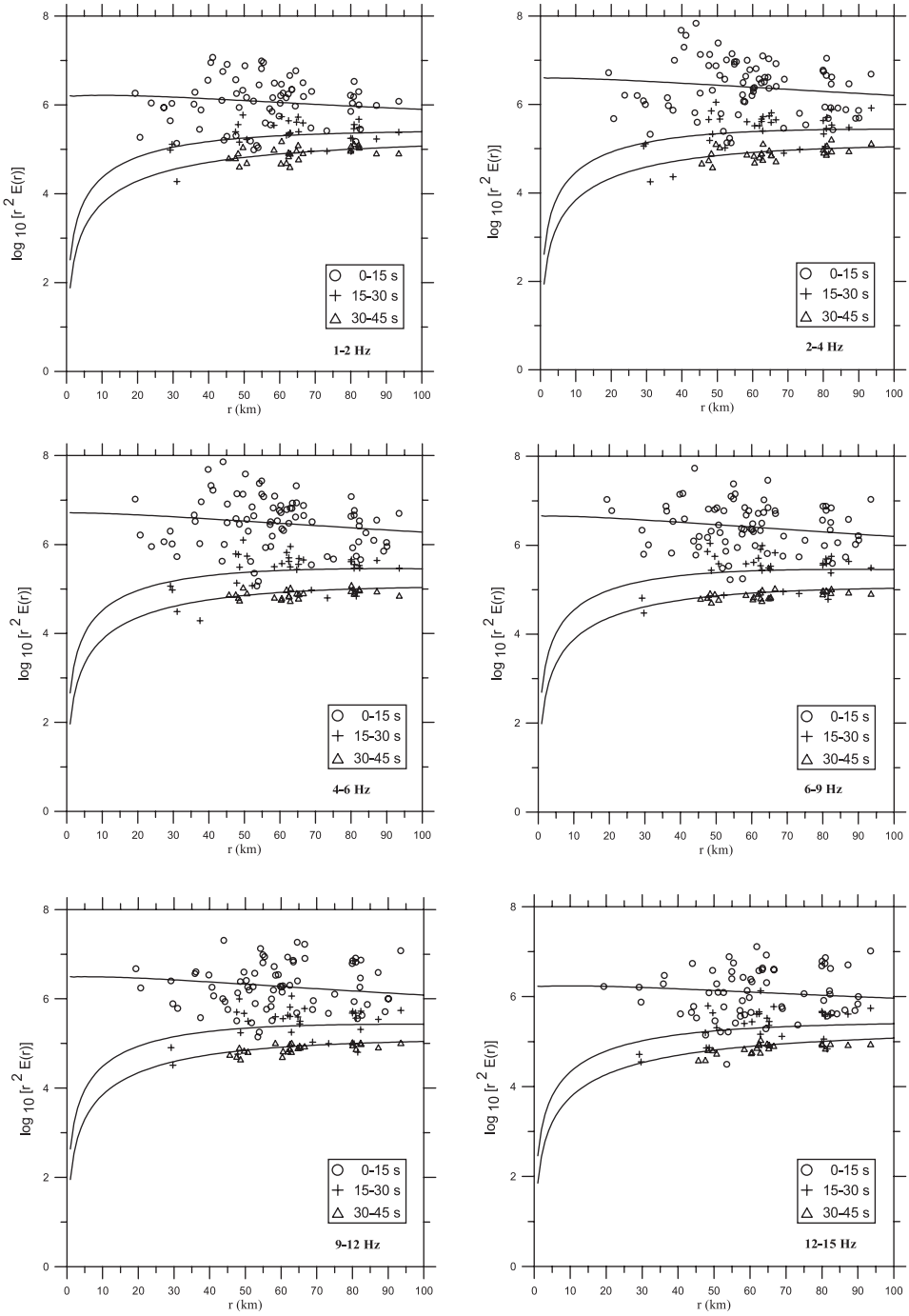

Figure 7. Plots of normalized energy ($\log_{10}[r^2E(r)]$) for the 1.5, 3, 5, 7.5, 10.5, and 13.5 center frequencies. Circles, triangles, and crosses represent the observed seismic energies integrated over the 0–15, 15–30, and 30–45 s time windows after the *S* arrival, respectively. The solid lines represent the synthetic energy curves best fitting the observed data.

intrinsic absorption and scattering contribute in equal shares to total attenuation for the 3, 5, 7.5, and 10.5 Hz center frequencies. As noted in section 4.4, these results represent the medium properties within a distance of ~100 km from each station. Figure 9 shows a comparative plot of Q_i^{-1}, Q_s^{-1}, Q_t^{-1}, and Q_c^{-1}. It is observed that Q_c^{-1} is close to Q_t^{-1} for the six analyzed center frequencies. As for the frequency dependence of the attenuation parameters, a decrease of around $1/f$ has been found for all the estimates. In terms of the random medium model, a decrease of Q_s^{-1} roughly inversely proportional to frequency is explained by a von Karman autocorrelation function of the medium of order 1/2 (that corresponds to the case of the exponential autocorrelation function) [*Sato*, 1982].

[24] Temporal and spatial variations in Q_c^{-1} have also being studied. The examination of a temporal change in Q_c^{-1} before and after the 25 January main shock has showed no significant variations for the six studied frequency bands between 1 and 15 Hz. However, a definite conclusion about the temporal change in Q_c^{-1}

Table 4. Inverse of the Extinction Length, Seismic Albedo, Intrinsic Absorption, Scattering Attenuation, and Total Attenuation for the Six Analyzed Frequency Bands

Center Frequency, Hz	L_e^{-1}, km^{-1}	B_0	$Qi^{-1} \times 10^3$	$Qs^{-1} \times 10^3$	$Qt^{-1} \times 10^3$
1.5	0.025+0.021 −0.015	0.64+0.08 −0.08	3.25	5.77	9.02
3.0	0.020+0.019 −0.011	0.48+0.12 −0.08	1.88	1.73	3.61
5.0	0.020+0.015 −0.011	0.44+0.10 −0.10	1.21	0.95	2.16
7.5	0.023+0.016 −0.012	0.48+0.10 −0.10	0.86	0.80	1.66
10.5	0.024+0.017 −0.014	0.54+0.08 −0.10	0.57	0.67	1.24
13.5	0.021+0.020 −0.013	0.62+0.14 −0.08	0.32	0.52	0.84

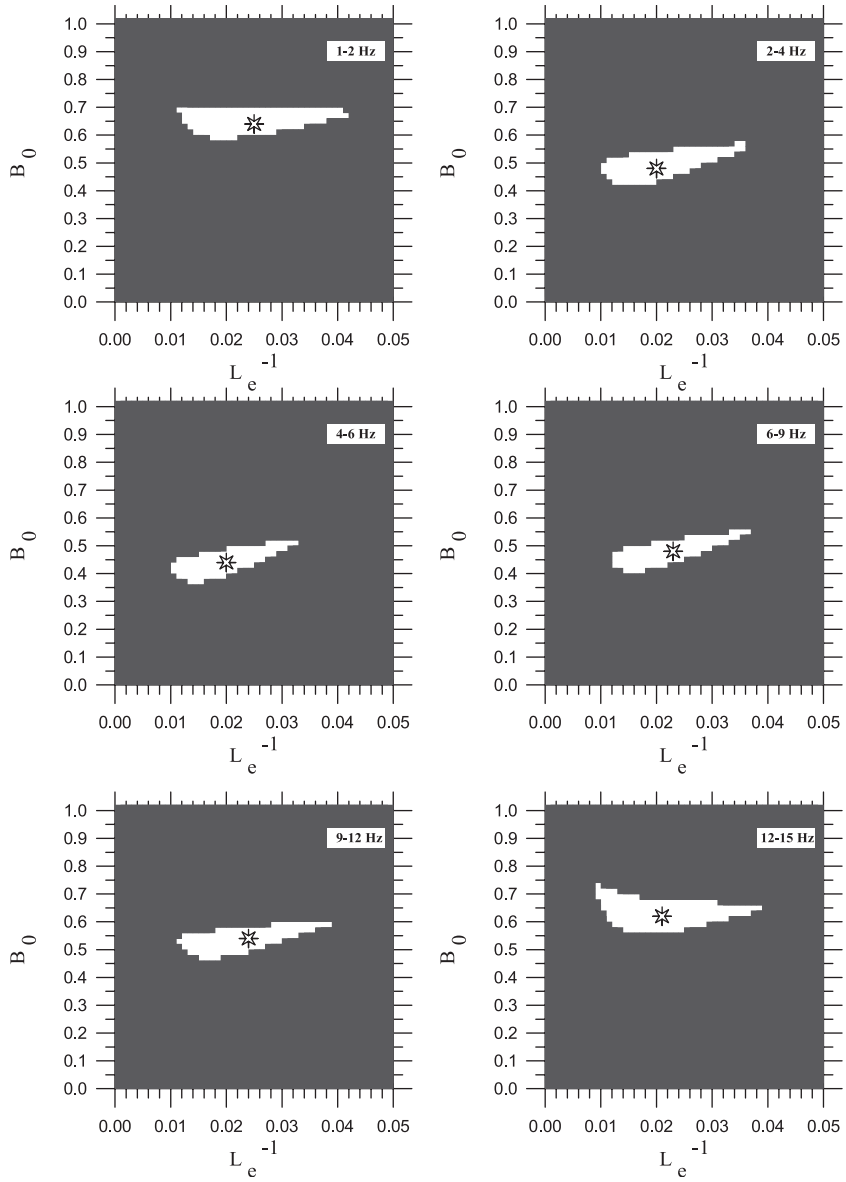

Figure 8. Confidence areas for the estimated model parameters, calculated by means of the *F* test for the six studied frequency bands. The symbols represent the pairs (L_e^{-1}, B_0) giving the minimum residual, and the unshaded areas are the 95% confidence regions.

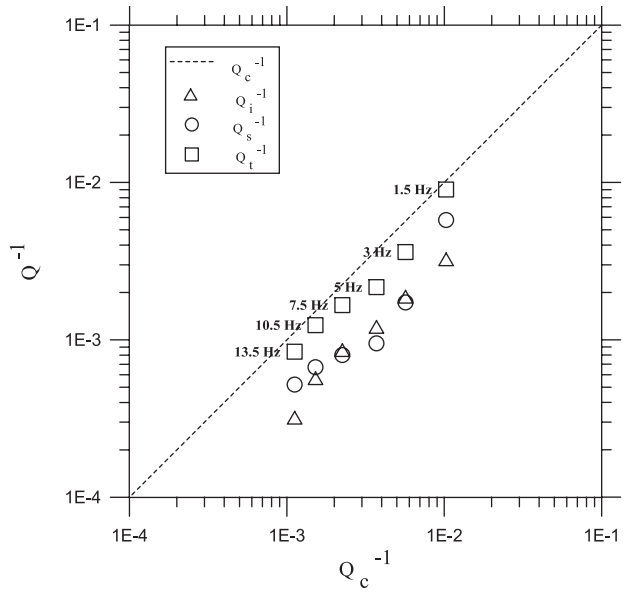

Figure 9. Comparison of the attenuation parameters Q_i^{-1}, Q_s^{-1}, and Q_t^{-1} with Q_c^{-1} for the six analyzed frequency bands between 1 and 15 Hz. Q_c^{-1} is closer to total attenuation for all the analyzed frequencies.

on the occasion of the Armenia earthquake is not possible due to the limited data available in this study.

[25] As for the spatial variation of Q_c^{-1}, no significant differences in the attenuation measurements for short and long hypocentral distances were observed. However, the distribution of data in this study does not allow to arrive to a definite conclusion about the spatial variation of Q_c^{-1} in the study area. Nevertheless, subregions with different Q values have been observed by plotting iso-Q maps for all the studied frequency bands using short lapse times. The method of regionalization used lies in assigning the Q_c^{-1} value estimated for each seismogram to the midpoint of the epicenter-station path. Despite the limited data available, a correlation between the estimated coda attenuation and the geological and tectonic environment can be performed. The central region of the Colombian Andes presents seismic and magmatic activity associated with shallow and intermediate tectonic processes. In general, the estimated seismic wave attenuation in this region is high which correlates well with the observed seismicity pattern [e.g., *Singh and Herrmann*, 1983; *Jin and Aki*, 1988]. On the other hand, from the geological point of view the study area for short lapse times may be divided into two zones from west to east: The Romeral faulting area and the Ruiz-Tolima volcanic complex (see Figure 2). Because the coda attenuation calculated at short lapse times is sensitive mainly to the crust, the Q_c values obtained are related to the observed geology of the region. From Figure 5 we see a zone of higher Q_c (low attenuation) located in the delimited area for the volcanic complex for the 3, 5, and 7.5 Hz center frequencies. Moreover, the highest attenuation (highlight zones in the figure) corresponds to the faulting area.

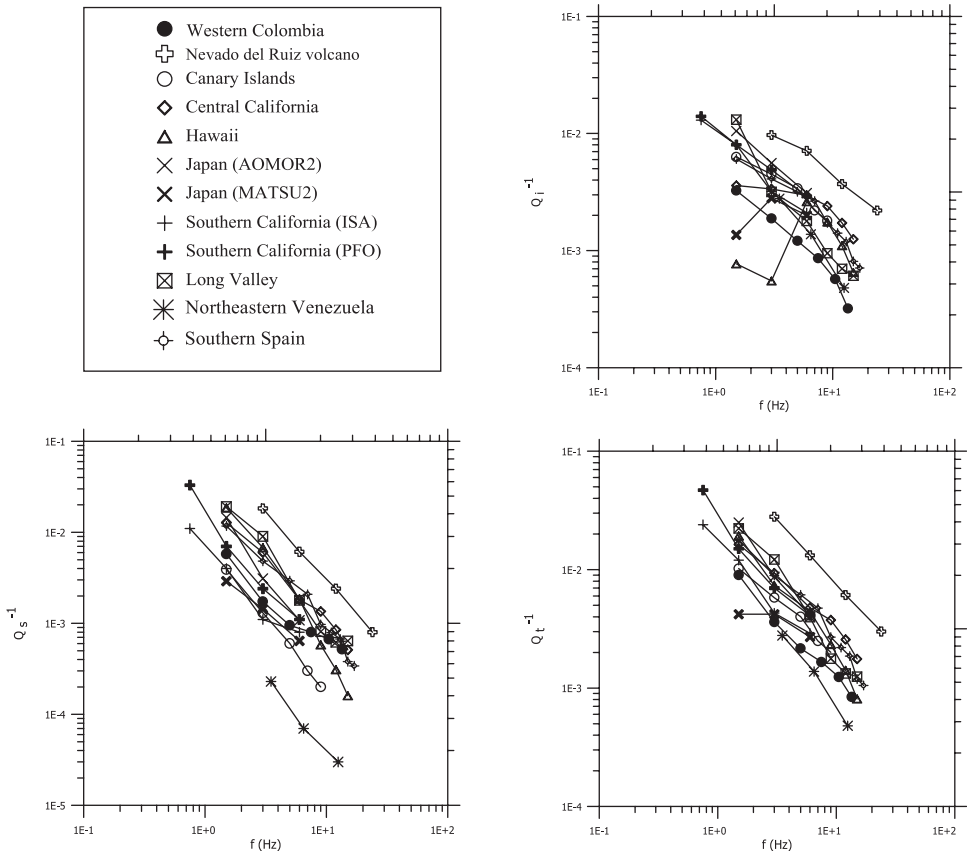

Figure 10. Comparison of Q_i^{-1}, Q_s^{-1}, and Q_t^{-1} as a function of frequency for different regions: This study; Nevado del Ruiz volcano [*Londoño*, 1996]; Canary Islands [*Canas et al.*, 1998]; central California, Long Valley, and Hawaii [*Mayeda et al.*, 1992]; Japan [*Hoshiba*, 1993]; southern California [*Jin et al.*, 1994]; northeastern Venezuela [*Ugalde et al.*, 1998]; and southern Spain [*Akinci et al.*, 1995].

[26] Finally, a regional comparison of the results of this study with the attenuation parameters estimated in other active areas around the world will be performed. As for Q_c^{-1}, *Ambeh and Lynch* [1993] studied the eastern Caribbean subduction zone using the *Sato* [1977] method and found that Q_0 varies from 97 to 145. Our results for long hypocentral distances show that $Q_0 = 44$, which implies that the attenuation is higher in the central region of the Colombian Andes. In this case, the earthquakes used are associated to the subduction of the Nazca plate beneath South America. On the other hand, to the best of our knowledge, the only attenuation studies carried out in this region are those of *Londoño* [1996] and *Londoño et al.* [1998], who calculated Q_c^{-1} in the specific zone of the Nevado del Ruiz volcano using the single-scattering method of *Aki and Chouet* [1975] and Q_i^{-1}, Q_s^{-1}, and Q_t^{-1} using the MLTW method of *Hoshiba et al.* [1991]. Londoño found that the scattering attenuation is the dominant attenuation process at low frequencies, whereas the intrinsic absorption is predominant for frequencies >6 Hz. Londoño's and our numerical results differ substantially which may be explained by the fact that *Londoño* [1996] *Londoño et al.* [1998] studied a very small area (around 25 km in diameter and 20 km in depth) centered at the Nevado del Ruiz volcano, whereas our study focuses on a larger region. Figure 10 summarizes a comparison among the estimated intrinsic, scattering, and total attenuation parameters in several regions of the world, where solid circles represent the results of this study. It can be seen that the Q_i^{-1}, Q_s^{-1}, and Q_t^{-1} estimates for the Nevado del Ruiz volcano are high in comparison with the other regions considered. From Figure 10 it is observed that total attenuation in the Colombian coffee-growing region is greater than the obtained for station MATSU2 in Japan and is similar to the Canary Islands estimate for the 1.5 center frequency. For the 3 Hz center frequency, our results are similar to Japan (MATSU2), southern California (station ISA), and northeastern Venezuela and are lower than for the other regions. The estimate of total attenuation for 5 and 7.5 Hz center frequencies in this study is also similar to and greater than the obtained in northeastern Venezuela, respectively, and lower than for the other regions. As for higher center frequencies, total attenuation in this study is similar to the estimates in Long Valley and Hawaii. The seismic albedo and thus the scattering attenuation coefficients are, in general, greater in western Colombia than in Japan (MATSU2), southern California (station ISA), the Canary Islands, and northeastern Venezuela for frequencies lower than 5 Hz. For higher frequencies the Q_s^{-1} parameter is similar to the obtained in Long Valley, central California, southern Spain, and southern California (ISA) and is greater than the estimated in the Canary Islands, Hawaii, and northeastern Venezuela. The intrinsic absorption in this study is greater than that calculated for the 1.5 Hz frequency in Japan (MATSU2) and Hawaii and is similar to the estimate in central California. For high frequencies the intrinsic absorption in the Colombian coffee-growing region is lower than the obtained in the other regions considered. These results mean that the central region of the Colombian Andes is more heterogeneous and more attenuating than Japan (MATSU2) and northeastern Venezuela on the scale length corresponding to the mentioned frequency ranges. However, our study region is, in general, more heterogeneous but less attenuating than southern California, Hawaii, and the Canary Islands.

[27] **Acknowledgments.** We gratefully acknowledge INGEOMINAS and Héctor Mora, Álvaro P. Acevedo, and César Carvajal for providing us with the data from Colombia. We greatly appreciate many constructive comments by K. Aki, the Associate Editor, and an anonymous reviewer for improving the manuscript. This paper has been partially supported by CICYT and DGES; projects AMB98-0558, and PB96-0139-C04-03.

References

Aki, K., Scattering and attenuation of shear waves in the lithosphere, *J. Geophys. Res.*, *85*, 6496–6504, 1980.

Aki, K., Scattering and attenuation, *Bull. Seismol. Soc. Am.*, *72*, 319–330, 1982.

Aki, K., Summary of discussions on coda waves at the Istanbul IASPEI meeting, *Phys. Earth Planet. Inter.*, *67*, 1–3, 1991.

Aki, K., and B. Chouet, Origin of coda waves: Source, attenuation and scattering effects, *J. Geophys. Res.*, *80*, 3322–3342, 1975.

Ambeh, W. B., and L. L. Lynch, Coda *Q* in the eastern Caribbean, West Indies, *Geophys. J. Int.*, *112*, 507–516, 1993.

Antolik, M., R. M. Nadeau, R. C. Aster, and T. V. McEvilly, Differential analysis of coda *Q* using similar microearthquakes in seismic gaps, part 2, Application to seismograms recorded by the Parkfield high resolution seismic network, *Bull. Seismol. Soc. Am.*, *86*, 890–910, 1996.

Aster, R. C., G. Slad, J. Henton, and M. Antolik, Differential analysis of coda *Q* using similar microearthquakes in seismic gaps, part 1, Techniques and application to seismograms recorded in the Anza seismic gap, *Bull. Seismol. Soc. Am.*, *86*, 868–889, 1996.

Canas, J. A., A. Ugalde, L. G. Pujades, J. C. Carracedo, V. Soler, and M. J. Blanco, Intrinsic and scattering seismic wave attenuation in the Canary Islands, *J. Geophys. Res.*, *103*, 15,037–15,050, 1998.

Coral, C. E., Los terremotos en Colombia y características de su origen profundo, Ph.D. thesis, Univ. Nac. de Colombia, Bogotá, 1987.

Dainty, A., A scattering model to explain seismic *Q* observations in the lithosphere between 1 and 30 Hz, *Geophys. Res. Lett.*, *11*, 1126–1128, 1981.

Draper, N. R., and H. Smith, Applied Regression Analysis, John Wiley, New York, 1981.

Fehler, M., M. Hoshiba, H. Sato, and K. Obara, Separation of scattering and intrinsic attenuation for the Kanto-Tokai region, Japan, using measurements of *S*-wave energy vs. hypocentral distance, *Geophys. J. Int.*, *108*, 787–800, 1992.

Herráiz, M., and A. F. Espinosa, Coda waves: A review, *Pure Appl. Geophys.*, *125*, 499–577, 1987.

Hiramatsu, Y., N. Hayashi, and M. Furumoto, Temporal changes in coda Q^{-1} and *b* value due to the static stress change associated with the 1995 Hyogo-ken Nanbu earthquake, *J. Geophys. Res.*, *105*, 6141–6151, 2000.

Hoshiba, M., Separation of scattering attenuation and intrinsic absorption in Japan using the multiple lapse time window analysis of full seismogram envelope, *J. Geophys. Res.*, *98*, 15,809–15,824, 1993.

Hoshiba, M., H. Sato, and M. Fehler, Numerical basis of the separation of scattering and intrinsic absorption from full seismogram envelope: A Monte-Carlo simulation of multiple isotropic scattering, *Pap. Meteorol. Geophys.*, *42*, 65–91, 1991.

Jin, A., and K. Aki, Spatial and temporal correlation between coda *Q* and seismicity in China, *Bull. Seismol. Soc. Am.*, *78*, 741–769, 1988.

Jin, A., and K. Aki, Spatial and temporal correlation between coda *Q* and seismicity and its physical mechanism, *J. Geophys. Res.*, *94*, 14,041–14,059, 1989.

Jin, A., K. Mayeda, D. Adams, and K. Aki, Separation of intrinsic and scattering attenuation in southern California using TERRAscope data, *J. Geophys. Res.*, *99*, 17,835–17,848, 1994.

Londoño, B. J. M., Temporal changes in coda *Q* at Nevado del Ruiz volcano, Colombia, *J. Volcanol. Geotherm. Res.*, *73*, 129–139, 1996.

Londoño, B. J. M., A. J. J. Sánchez, E. L. E. Toro, F. G. Cruz, and O. P. Bohórquez, Coda *Q* before and after the eruptions of 13 November 1985, and 1 September 1989, at Nevado del Ruiz volcano, Colombia, *Bull. Volcanol.*, *59*, 556–561, 1998.

Mayeda, K., S. Koyanagi, M. Hoshiba, K. Aki, and Y. Zeng, A comparative study of scattering, intrinsic and coda Q^{-1} for Hawaii, Long Valley, and central California between 1.5 and 15.0 Hz, *J. Geophys. Res.*, *97*, 6643–6659, 1992.

Muñoz, F. A., Local earthquake tomography for lateral velocity variations and hypocenters at Nevado del Ruiz volcano, Colombia, Ms. thesis, Ariz. State Univ., Tempe, 1992.

National Earthquake Information Center, Preliminary determination of epicenters, *U.S. Geol. Surv.*, Denver, Colo., 1999.

Pujades, L. G., A. Ugalde, J. A. Canas, M. Navarro, F. J. Badal, and V. Corchete, Intrinsic and scattering attenuation from observed seismic codas in the Almeria Basin (southeastern Iberian peninsula), *Geophys. J. Int.*, *129*, 281–291, 1997.

Pulli, J. J., Attenuation of coda waves in New England, *Bull. Seismol. Soc. Am.*, *74*, 1149–1166, 1984.

Rautian, T. G., and V. I. Khalturin, The use of coda for determination of the earthquake source spectrum, *Bull. Seismol. Soc. Am.*, *68*, 923–948, 1978.

Sato, H., Energy propagation including scattering effects; single isotropic scattering, *J. Phys. Earth*, *25*, 27–41, 1977.

Sato, H., Attenuation of *S* waves in the lithosphere due to scattering by its random velocity structure, *J. Geophys. Res.*, *87*, 7779–7785, 1982.

Sato, H., Multiple isotropic scattering model including *P*–*S* conversions

from the seismogram envelope formation, *Geophys. J. Int.*, *117*, 487–494, 1994.

Singh, S., and R. B. Herrmann, Regionalization of crustal coda *Q* in the continental United States, *J. Geophys. Res.*, *88*, 527–538, 1983.

Taboada, A., C. Dimaté, and A. Fuenzalida, Sismotectónica de Colombia: deformación continental activa y subducción, *Fís. Tierra*, *10*, 111–147, 1998.

Ugalde, A., L. G. Pujades, J. A. Canas, and A. Villaseñor, Estimation of the intrinsic absorption and scattering attenuation in northeastern Venezuela (southeastern Caribbean) using coda waves, *Pure Appl. Geophys.*, *153*, 685–702, 1998.

Wu, R. S., Multiple scattering and energy transfer of seismic waves: Separation of scattering effect from intrinsic attenuation, I, Theoretical modelling, *Geophys. J. R. Astron. Soc.*, *82*, 57–80, 1985.

Zeng, Y., F. Su, and K. Aki, Scattered wave energy propagation in a random isotropic scattering medium, I, Theory, *J. Geophys. Res.*, *96*, 607–619, 1991.

J. A. Canas, Instituto Geográfico Nacional, General Ibáñez de Ibero, 3, 28003-Madrid, Spain. (jacanas@mfom.es)

L. G. Pujades, Universitat Politècnica de Catalunya, Dep. Enginyeria del Terreny i Cartogràfica, Gran Capità, s/n, D-2, E-08034-Barcelona, Spain. (lluis.pujades@upc.es)

A. Ugalde, Observatori de l'Ebre, Horta Alta, 38, E-43520-Roquetes, Spain. (ebre.augalde@readysoft.es)

C. A. Vargas, Ingeominas, Av. 12 de Octubre, 15–47, Manizales, Colombia. (cavj@hotmail.com)

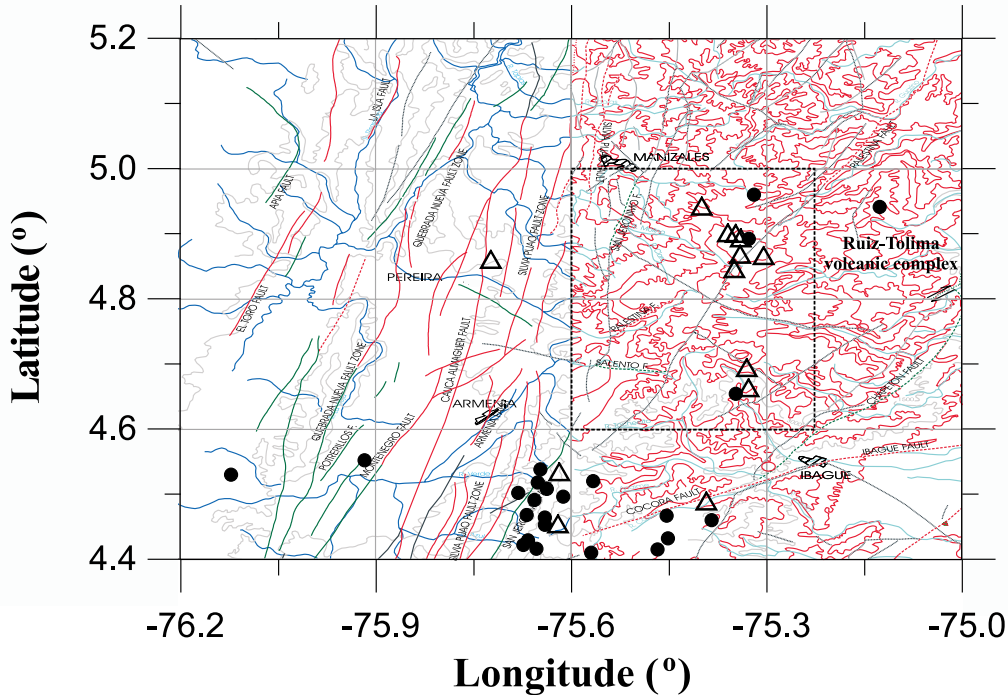

Figure 2. Detailed map of part of the studied region. The main faults and the location of the Ruiz-Tolima volcanic complex (rectangular area surrounded by dashed square) are shown together with the location of some of the stations (triangles) and earthquakes (solid circles) used.